

OPEN ACCESS

EDITED BY Zeynep Eren, Atatürk University, Türkiye

REVIEWED BY Zeynep Zaimoglu, Cukurova University, Türkiye Başak Savun, Istanbul University, Türkiye

*CORRESPONDENCE Habibullah Uzun, ⊠ uzunh@itu.edu.tr

RECEIVED 06 July 2025 ACCEPTED 18 August 2025 PUBLISHED 01 September 2025

CITATION

Uzun H (2025) The impact of ash-derived natural organic matter on the adsorption of MIB and geosmin by powdered activated carbon. *Front. Environ. Sci.* 13:1660425. doi: 10.3389/fenvs.2025.1660425

COPYRIGHT

© 2025 Uzun. This is an open-access article distributed under the terms of the Creative Commons Attribution License (CC BY). The use, distribution or reproduction in other forums is permitted, provided the original author(s) and the copyright owner(s) are credited and that the original publication in this journal is cited, in accordance with accepted academic practice. No use, distribution or reproduction is permitted which does not comply with these terms.

The impact of ash-derived natural organic matter on the adsorption of MIB and geosmin by powdered activated carbon

Habibullah Uzun 📵 *

Department of Environmental Engineering, Istanbul Technical University, Istanbul, Türkiye

Wildfires substantially alter watershed chemistry, increasing natural organic matter (NOM) loads and nutrient fluxes into surface waters, which can stimulate algal blooms and the production of taste and odor (T&O) compounds such as 2-methylisoborneol (MIB) and geosmin. This study investigated the performance of five commercially available powdered activated carbons (PACs) in removing MIB and Geosmin from water impacted by ash-derived NOM. Adsorption experiments were conducted using NOM-free water and wildfire-generated white-ash leachate (WA-L), black-ash leachate (BA-L), and unburned vegetation leachate (UV-L), each with 7.5 mg/L DOC and varying aromaticity and molecular weights (MW) (as indicated by SUVA₂₅₄ and E2/E3 ratios). Under NOM-free conditions, PACs with significant micropore volumes exhibited exceptional adsorption capabilities. PAC-4, distinguished by its narrow micropores (~0.15 cm³/g in the 0.54-1 nm range) and high pHpzc (8.7), exhibited the highest uptake of both compounds. The adsorption kinetics revealed that within 60 min, over 80% of MIB and 90% of geosmin were removed by all the carbons. PACs with well-balanced microporosity exhibited the most rapid initial uptake (10-30 min). Under NOM conditions, UV-L led to significant pore blocking because of the presence of high-MW NOM. In contrast, WA-L, which contains smaller and more hydrophobic NOM, caused minimal suppression. Despite NOM suppression, a PAC dose of 20 mg/L enabled all PACs (except mesoporous carbon) to achieve ≥85% MIB and ≥98% geosmin removal in WA-L and partially in BA-L. These results highlight the importance of selecting PACs based on pore structure and surface chemistry, as well as the need to adjust PAC dosage during post-wildfire events.

KEYWORDS

wildfires, ash-derived NOM, MIB and geosmin, PAC, adsorption

1 Introduction

2-Methylisoborneol (MIB) and Geosmin are naturally occurring organic compounds that impart earthy and musty odors to water. These compounds are primarily produced by cyanobacteria (known as blue-green algae) and actinobacteria, particularly during algal blooms in nutrient-rich freshwater environments (Doederer et al., 2018; Matsui et al., 2013; Newcombe et al., 2002a). Their production is influenced by various factors, such as the composition of microbial communities, temperature, nutrient availability and fluxes, and light intensity in the aquatic environment (Kim and Park, 2021; Lee et al., 2020; Otten et al., 2016; Qiu et al., 2023). The concentrations of MIB and Geosmin in water sources can exceed 100 ng/L under bloom conditions (Doederer et al., 2018; Lee et al., 2020; Watson et al.,

2000). Due to their extremely low odor thresholds (4 ng/L for Geosmin and 15 ng/L for MIB), even trace levels that are not removed during water treatment may lead to consumer complaints (Kim and Park, 2021; Lee et al., 2020; Otten et al., 2016; Srinivasan and Sorial, 2011; Szczurek et al., 2024). However, their small and stable bicyclic monoterpene structure with moderate water solubility contributes to their resistance against conventional treatment processes such as coagulation, flocculation, sedimentation, filtration, and oxidations with either chlorine (Cl₂) or chlorine dioxide (ClO₂) (Antonopoulou et al., 2014; Cerón-Vivas et al., 2023; Mustapha et al., 2021; Qiu et al., 2023; Srinivasan et al., 2008; Srinivasan and Sorial, 2011; 2009a). Consequently, effective removal of these compounds often requires advanced and costly methods, including ozonation, advanced oxidation processes (AOPs), membrane filtration, and carbon adsorption (Doederer et al., 2018; Klausen and Grønborg, 2010; Matsui et al., 2007; Westerhoff et al., 2006). Among these, powdered activated carbon (PAC) is the most widely used technique worldwide for eliminating MIB and Geosmin from treated drinking water (Cerón-Vivas et al., 2022; Park et al., 2010; Pochiraju et al., 2022; Srinivasan and Sorial, 2011). However, the presence of dissolved organic matter (DOM) in source water can hinder PAC's performance by competing for adsorption sites or blocking access to the PAC's pores (Cook and Newcombe, 2004; Newcombe et al., 2002a; Srinivasan and Sorial, 2009b).

Wildfires are a major ecological disturbance, often leading to significant shifts in nutrient dynamics. These events can significantly enhance the export of nitrogen and phosphorus to water bodies via ash deposition, increased soil erosion, and hydrological alterations (De Palma-Dow et al., 2022; Emelko et al., 2011; Feller, 2005; Gustine et al., 2022; Hampton et al., 2022; Silins et al., 2009). Research has shown that elevated nutrient levels can persist in affected water sources for extended periods, increasing the likelihood of eutrophication, particularly in warm, stratified reservoirs with adequate light availability (Gleasman et al., 2025; Paul et al., 2022; Richardson et al., 2024; Tsai et al., 2017). Postfire ash transport poses further challenges by altering the composition of DOM (i.e., black and white ash-derived DOMs) in receiving waters, potentially stimulating algal growth when combined with nutrient influx (Blackburn et al., 2023; Campbell et al., 2024; Chen et al., 2021; Ferrer et al., 2021; Tsai et al., 2019; 2017).

Given the increasing frequency of wildfires and their potential impact on nutrient levels and changes in DOM composition in water sources, it is essential to assess the effectiveness of PACs in removing MIB and Geosmin when ash-derived DOM is present in raw water. Although many studies have evaluated MIB and geosmin adsorption under various water qualities, none have specifically investigated PAC adsorption performance in the presence of wildfire ash-derived NOM, leaving water utilities uncertain about the continued efficacy of PACs during postfire algal bloom events. Therefore, this study aimed to assess the effectiveness of commercially available and widely used PACs with different characteristics in removing MIB and Geosmin from water containing black and white ash-derived DOM. This study is the first to explore how ash leachates, characterized by their distinct MW and aromaticity, interact with PACs that differ in their pore structure and surface chemistry. These findings are crucial for understanding the challenges associated with post-wildfire water treatment. The findings of this study aim to assist water utilities in optimizing their treatment strategies to effectively remove MIB and Geosmin from water following wildfire events.

2 Materials and methods

2.1 Wildfires, unburned vegetation and ash collection

Sonomo-Lake-Napa Unit (LNU) Lightning Complex fires were ignited by several lightning strikes during the wildfire season (August-October 2020) in California (CA) and impacted five counties. The fires consumed approximately 363,200 acres and were contained on October 1 (NICC, 2020). Based on the vegetation data and analysis results, most parts of the sample collection areas (the western part of Napa County, which has mostly oak woodlands and shrublands) for this study were assumed to be exposed to moderate-to high-intensity and severe fires (Marden, 2020), forming black ash with incomplete burning and white ash with complete burning (Campbell et al., 2024). To test the objective of this study, black and white ash samples were collected following the containment of the fire at the Quail Ridge Natural Reserve, Napa County. Around 1 kg of samples (black ash [BA] and white ash [WA]) were obtained from the central location (38 28.945' N 122 8.866'W), with an additional 5 kg of solid samples gathered from approximately a 50-m radius surrounding this central point in the northern, southern, eastern, and western directions, and subsequently mixed thoroughly. Furthermore, litter, identifiable plant parts, and duff materials were collected from nearby unaffected landscape sections as unburned vegetation (UV) and mixed thoroughly. After collection, the solid samples were dried in an oven at 30 °C for 72 h and stored in moisture-free containers until use.

2.2 Leaching experiments and water quality tests

Following a series of preliminary leaching experiments to determine the correct solid application dose, a pre-determined amount of solid samples was immersed in a B-KER2 Laboratory Test Jar (Phipps and Bird-PHIPPS), including 2 L of distilled and deionized water (DDW) for 24 h at 100 rpm to produce UV-derived leachate (UV-L), black ash-derived leachate (BA-L), and white ashderived leachate (WA-L) waters (Supplementary Figure S1), each with a targeted dissolved organic carbon (DOC) content of 7.5 \pm 0.1 mg/L. Subsequently, the leachates were filtered using pre-washed Whatman Glass filters with a filter diameter of 10 cm (pore size of approximately 0.7 µm) and PAL Supor PES membrane filters with a pore size of approximately 0.45 µm. Following filtration, water quality (WQ) tests were conducted to measure dissolved organic carbon (DOC), dissolved nitrogen (DN), UV254, SUVA254 (which indicates the hydrophobicity of the water), and E2/E3 (which is inversely related to the molecular weight [MW] of the compounds). These tests and calculations were performed using methodologies previously established and documented in the literature (Chen et al., 2023; Majidzadeh et al., 2020; Majidzadeh et al., 2019; Uzun et al., 2019; Uzun et al., 2018). Table 1 summarizes the yields, expressed as

TABLE 1 Leaching yields and comparison of raw water quality parameters of leachate waters.

Leachate Waters	Leaching (mg DOC or D material in	N/gram solid	Water quality parameters in DOC-adjusted waters used for adsorption tests					
	DOC (mg/L)	DN (mg/L)	DOC (mg/L)	DN (mg/L)	SUVA ₂₅₄ (L/mg-m)	E2/E3		
UV-L	21.73 ± 3.42	8.26 ± 1.22	7.52 ± 0.10	2.85 ± 0.14	2.22 ± 0.04	5.6 ± 0.05		
BA-L	3.81 ± 0.31	1.14 ± 0.11	7.51 ± 0.08	2.24 ± 0.11	2.66 ± 0.03	8.5 ± 0.04		
WA-L	1.33 ± 0.06	0.39 ± 0.02	7.45 ± 0.08	2.16 ± 0.08	3.38 ± 0.02	13.5 ± 0.05		

Leaching Conditions: A pre-determined amount of dry solid material was agitated in DDW, for 24 h at a mixing rate of 100 rpm. Subsequently, the samples underwent filtration using 0.7 µm glass filters and 0.45 µm PES, membrane filters, respectively. UV-L, unburned vegetation-derived leachate, BA-L, black ash-derived leachate, and WA-L, white ash-derived leachate waters.

milligrams of DOC and DN per gram of solid material, along with the WQ parameters of the leachate utilized for subsequent adsorption tests, as detailed in Section 2.5.

2.3 Adsorbent preparation and characterization

Five commercially available and widely utilized activated carbons for water treatment were selected for this study. The adsorbents were obtained from three different Carbon Corporations in the United States (US) as granular activated carbons (GACs), which were produced from distinct materials, namely, wood, bituminous coal, and lignite coal. Before application to the solution, the GACs were ground and sieved through a Micro Sieve Shaker kit to obtain PACs with a particle size range of 44-74 µm (mesh size of 200-325) and named PAC-1, PAC-2, PAC-3, PAC-4, and PAC-5. Subsequently, the PACs were rinsed with DDW in 1-L glass beakers, with stirring maintained at 20 rpm. Any light PACs that remained suspended in the water were removed daily, and the discarded volume of water was replenished in the beaker for the seven-day rinsing period. The supernatant was then decanted, and the PACs were dried in an oven at 104 °C for 48 h. Subsequently, the adsorbents were cooled and stored in glass bottles within a vacuum desiccator until use (i.e., adsorbent characterization and adsorption experiments).

PACs' surface area and pore characteristics (i.e., pore volumes [cm³/g] and pore size distributions) of the PACs were measured using 70 points of nitrogen adsorption at 77.5 °K from a pressure of 10⁻⁶ to 1. Before nitrogen adsorption analysis, ~100 mg of pre-dried and sieved samples were degassed at 300 °K for 10 h using an ASAP 2020 analyzer from Micromeritics Instrument Corp. (US). The specific surface area (SSA) was determined using the Brunauer–Emmett–Teller (BET) equation. Simultaneously, the pore size distribution (between 5–600 Å or 0.5–60 nm) of the PAC samples was derived from the nitrogen isotherms via Density Functional Theory (DFT) (Dastgheib et al., 2004; Gagliano et al., 2021).

To determine the point of zero charge (pHpzc) of the PACs, 5 L of 0.1 M NaCl solution was prepared using DDW. Subsequently, 1 L aliquots were separated, and the pH of each was adjusted to 3, 5, 7, 9, and 11 using NaOH and HCl. Then, 250 \pm 0.1 mg of PACs was added to 50 mL of water, resulting in a 5 g-carbon/L concentration. These samples were agitated for 48 h at 100 rpm at room

temperature, followed by a 12-h settling period. The pH of the samples was measured using PAC-added and carbon-free solutions. The pHpzc of the adsorbents was determined at the pH where the values of the carbon-free and the PAC-containing solutions were identical (Supplementary Figure S2) (Dastgheib et al., 2004; Gagliano et al., 2021). Table 2 summarizes the carbon feedstock material type, pHpzc, BET SSA, and DFT pore volume distribution for different pore openings.

2.4 Chemicals and detection of MIB and geosmin

The standards of MIB were characterized as a white crystalline powder, and Geosmin, a liquid ranging from colorless to slightly yellow, was obtained from FUJIFILM Wako Pure Chemical Corporation. Supplementary Table S1 summarizes the key physical and chemical properties of MIB and Geosmin. Geosmind₃, a neat standard with an MW of 185.32 g/mol, was obtained from Millipore Sigma. Initially, primary dilution stocks (PDS) of 10 µg/L were prepared by adding a predetermined amount of chemicals to 10 mL of DDW. Subsequently, a predetermined quantity of the mixture was introduced into glass Phase Microextraction (SPME) vials containing 10 mL of DDW and 3 g of NaCl to achieve calibration standards ranging from 0.625 to 160 ng/L (nine points: 0.625, 1.25, 2.5, 5, 10, 20, 40, 80, and 160 ng/L). Additionally, 100 ng/L of Geosmin-d3 was spiked into all calibration and other samples as an internal standard for GC-MS analysis. Owing to the volatile nature of the target compounds, the samples were sealed with metal screw caps covered by PTFE/silicon septa (Ariturk, 2021).

All extractions were conducted using a PAL automated SPME fiber assembly, 50/30 μm DVB/CAR/PDMA from Millipore Sigma. An Agilent 7890B gas chromatograph coupled with a 7000C Triple Quadrupole mass spectrometer was used to quantify MIB and Geosmin. The injector was operated at 250 °C in splitless mode. A 30 m \times 0.25 mm ID×0.25 μm HP-5MS column was used for the separation. The temperature program commenced at 40 °C, maintained for 2 min, then increased to 220 °C at a rate of 20 °C/min, and held for 4 min. The transfer line temperature was maintained at 250 °C. Tandem mass spectrometry analysis employed electron ionization (EI), and the target compounds were quantified in multiple reaction monitoring (MRM) mode. Details regarding the GC/MSMS analysis, detection levels (DL), and minimum reporting

TABLE 2 Characteristics of PACs.

Carbons	Feedstock	pHpzc	BET	Units DFT pore volume distribution for specific pore openings (nr							(nm)	
Material type		m²/g	nm	<0.54	<0.54-1.0	1–2	2-10	10-20	20-50	>50	Total	
PAC-1	Wood	6.9	1708	cm³/g	0.0856	0.0285	0.2724	0.7935	0.1538	0.0376	0.000	1.37
PAC-2	Bituminous Coal	5.8	977		0.0184	0.0786	0.1925	0.1314	0.0074	0.0035	0.000	0.49
PAC-3	Bituminous Coal	9.7	774		0.0576	0.1007	0.1182	0.1183	0.0188	0.0080	0.000	0.42
PAC-4	Bituminous Coal	8.7	822		0.0260	0.1512	0.1443	0.0454	0.0090	0.0012	0.000	0.37
PAC-5	Lignite Coal	5.9	523		0.0536	0.0300	0.0623	0.1911	0.0904	0.0688	0.067	0.56

N/D, not detected.

levels (MRL) for MIB and Geosmin tests have been previously published (Ariturk, 2021; Soyluoglu et al., 2022; Soyluoglu, 2023). During GC/MSMS analysis, spike samples of 100 ng/L MIB and 100 ng/L Geosmin in DDW were analyzed after nine-point calibrations and every 20 to 25 samples, yielding average \pm SD concentrations of 100 \pm 9 ng/L for MIB and 100 \pm 6 ng/L for geosmin (n = 32).

2.5 Adsorption experiments

To determine the equilibrium uptakes of MIB and Geosmin from organic matter-free DDW and leachate waters, varying doses of PACs—specifically 3, 5, 10, 20, and 40 mg/L—were introduced into solutions (i.e., DDW [NOM-free], UV-L, BA-L, and WA-L) containing 250 \pm 5 ng/L of MIB and 250 \pm 5 ng/L Geosmin. Equilibrium was achieved after 72 h of mixing at 150 rpm in amber glass bottles with a sample volume of 125 mL. After contact, the samples were filtered using 0.2- μ m membrane filters to remove carbon from the solutions. Final MIB and Geosmin were determined using GC/MS-MS (described in Section 2.4), and the uptake was calculated using Equation 1.

$$qe = \frac{V (Co - Ce)}{m}$$
 (1)

Where Qe represents the adsorption capacity (ng/mg-carbon), and V and m denote the solution volume (mL) and adsorbent dose in solution (mg), respectively. The symbols Co and Ce correspond to the initial and final concentrations of the adsorbates in the solution, respectively, and are expressed in ng/L.

To evaluate the removal kinetics, 20 mg/L of PACs were introduced into 125 mL of NOM-free water (DDW) and leachate waters (UV-L, BA-L, and WA-L), each containing 100 ± 5 ng/L of MIB and 100 ± 5 ng/L of geosmin. Liquid samples were collected at intervals of 10, 30, 60, 90, and 120 min after PAC addition, and the concentrations of Ce were measured as previously described. Subsequently, the percent removal was calculated using Equation 2.

Removal,
$$\% = \frac{\text{(Co - Ce)}}{Co} \times 100$$
 (2)

To further quantify the adsorption kinetics, the pseudo-firstorder (PFO) kinetic model was employed to describe the timedependent concentration changes of MIB and geosmin. The PFO model was selected for its efficacy in capturing diffusion-limited characteristics of MIB and geosmin adsorption onto PAC. It demonstrated superior statistical fits and provided mechanistically interpretable rate constants compared to alternative models. The model assumes that the adsorption rate is proportional to the number of unoccupied adsorption sites and is commonly used to describe physical adsorption. Mathematically, the PFO model is represented as:

$$Ce = Co.e^{-kt}$$
 (3)

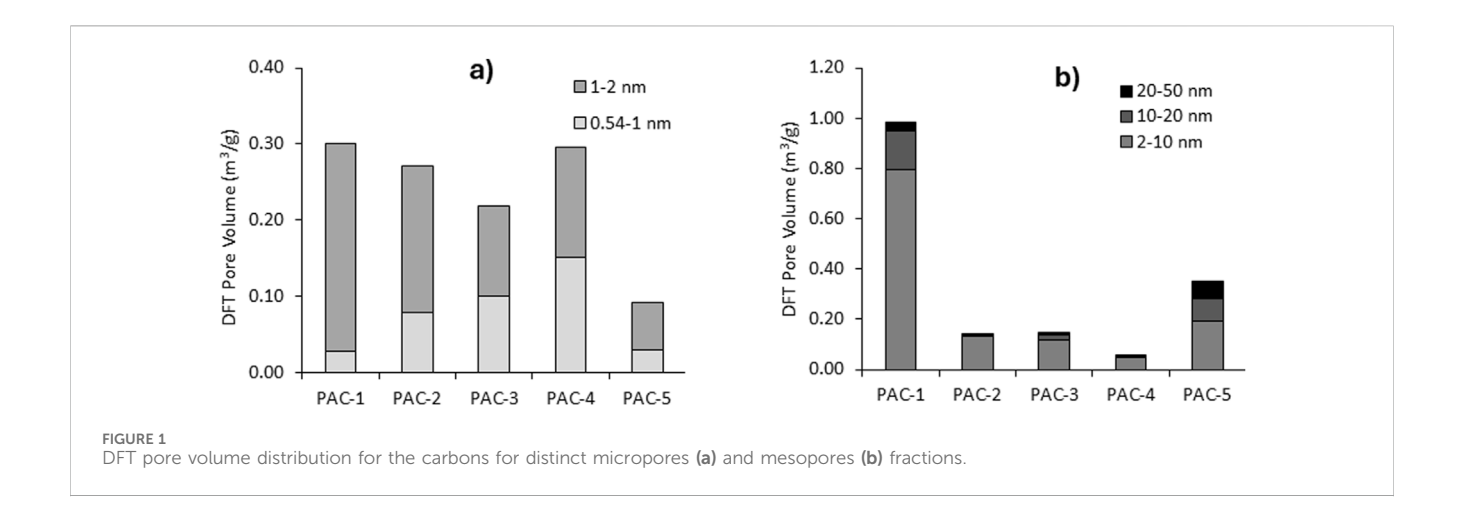
where Ce represents the aqueous-phase concentration (ng/L) at time t (min), Co denotes the initial concentration (ng/L), k is the PFO rate constant (min^{-1}), and t is the contact time (min). For further details of the analysis, please refer to the SI.

One limitation is that adsorption isotherms and kinetic profiles were measured once per isotherm or kinetic test, preventing statistical analyses such as ANOVA or t-tests. This design choice was necessary given the extensive experimental matrix, which included over 240+ isotherms and 240+ kinetic points, along with 700+ Quality Assurance and Quality Control (QA/QC) and calibration samples (please refer to Section 2.4). However, to ensure data reliability, rigorous QA/QC protocols were implemented, and trends were assessed through model fitting (e.g., isotherm models and pseudo-first-order kinetics) and descriptive comparisons.

3 Results and discussion

3.1 Water quality of leachate waters

The levels of DOC (21.73 \pm 3.42) and DN (8.26 \pm 1.22) measured in UV-L were significantly higher (p < 0.05), yielding mg DOC or DN per gram of solid material in 1 L DDW, compared to the ash leachates (Table 1): BA-L and WA-L yields were 3.81 \pm 0.31 and 1.33 \pm 0.06 for DOC, and 1.14 \pm 0.11 and 0.39 \pm 0.02 for DN, respectively. This suggests that wildfire combustion diminishes the mass of water-extractable dissolved organic matter (WE-DOM). The degree of combustion completeness, often indicated by white ash, is associated with greater losses in WE-DOM. This is because high-severity fires tend to volatilize or oxidize organic compounds, resulting in ash that is richer in minerals and poorer in DOM (Bodí et al., 2014; Chen et al., 2022; 2020; Tsai et al., 2017). As previously mentioned, the DOC content was adjusted to 7.5 \pm 0.1 mg/L (generally, 2–10 mg/L DOC is present in natural water). (Cook



et al., 2001; Cook and Newcombe, 2004). used DDW to evaluate the adsorption efficiency of PACs. Consequently, the DN content was measured proportionally (Table 1). In these waters, the SUVA₂₅₄ value for BA-L was higher than that for UV-L, whereas white ash exhibited the highest value. Additionally, the E2/E3 value for black ash exceeded that of the unburned material, with white ash exhibiting the highest value. Higher SUVA₂₅₄ values in black and white ash indicated increased aromaticity, whereas higher E2/ E3 ratios suggested a reduction in the MW of DOM. This reflects fire-induced aromatic condensation and the molecular fragmentation of DOM. (Chen et al., 2020; Weishaar et al., 2003). Therefore, these results indicate that the MW of DOMs follows the order UV-L > BA-L > WA-L. In the subsequent sections, a critical evaluation and discussion will be conducted on the removal of MIB and Geosmin, considering the properties of PACs (Table 2), the relative aromaticity of DOM, and the proposed MW orders.

3.2 Adsorbents

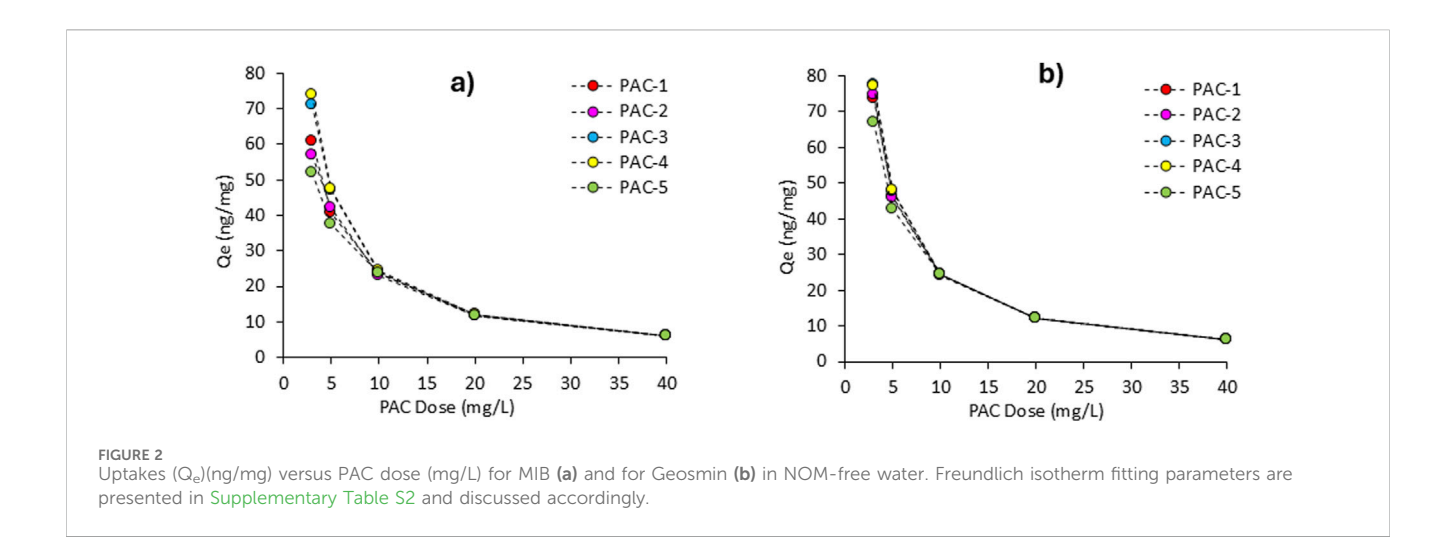
PAC-1, derived from wood, demonstrated the highest BET surface area (~1708 m²/g) and total pore volume (~1.37 cm³/g) (Table 2). Its porosity is predominantly mesoporous (~0.98 cm³/g) with a significant microporous fraction (~0.39 cm³/g). In contrast, PAC-2 and PAC-3, sourced from bituminous coal, exhibited substantial microporosity (~0.29 and ~0.28 cm³/g, respectively) and moderate mesoporosity (~0.14 and 0.15 cm³/g). PAC-4 also displayed high microporosity (~0.32 cm³/g) but limited mesoporosity (<0.06 cm³/g). PAC-5, derived from lignite coal, was characterized by prominent mesoporosity (~0.35 cm³/g), although its microporosity was relatively low. Given the importance of micropores in the adsorption of MIB and Geosmin, DFT pore volume distributions were further examined. For pores in the 1-2 nm range (10-20 Å), the ranking was PAC-1 > PAC-2 > PAC-4 > PAC-3 > PAC-5. For the narrower 0.54–1 nm range [as the target compounds cannot enter pores smaller than 0.50 nm (Supplementary Table S1), and the instrumental method measures 0.54 nm, which is the closest size to 0.50 nm, this range was chosen], the order was PAC-4 > PAC-3 > PAC-2 > PAC-5 ~ PAC-1 (Figure 1a). These trends highlight the heterogeneity in PAC structures and their potential efficacy in the removal of small MIB and Geosmin compounds, with BET areas ranging from 523 to 1708 m^2/g and DFT pore volumes for micropores (Figure 1a) and mesopores (Figure 1b) spanning 0.04–0.39 cm³/g and 0.05–0.98 cm³/g, respectively. The pH_{pzc} values varied from 5.8 to 9.7 for the adsorbents (Table 2).

Consequently, as previously described, adsorption experiments were conducted using NOM-free, UV-L, BA-L, and WA-L to assess the objectives. The adsorbent dosage was varied to determine the uptake while keeping the adsorbate concentration constant, with calculations performed as previously explained. This approach aimed to ensure that the PAC dosage for the kinetic experiments was determined based on experimental results rather than arbitrarily. Thus, adsorption uptake was evaluated by varying the adsorbent dose from 3 to 40 mg/L while maintaining MIB and Geosmin concentrations at 250 \pm 5 ng/L. The Freundlich isotherm (SI), which accommodates multilayer adsorption, is particularly effective at the low concentrations typically encountered in drinking water applications (Kim et al., 2014; Matsui et al., 2013; Newcombe et al., 2002b). Although both Langmuir and the Freundlich isotherm models were evaluated in this study, the discussion focuses on the Freundlich isotherm fitting parameters because of their superior performance, which aligns with the existing literature (Bong et al., 2021; Matsui et al., 2013).

3.3 MIB and geosmin uptake in NOM-Free water

The results indicate distinct trends in adsorption performance, which can be attributed to the collective interactions between the accessible pore volume, surface area, and surface chemistry (Belhachemi, 2021). Despite both compounds (i.e., MIB and Geosmin) being hydrophobic, low in MW, and neutral under experimental conditions, subtle differences in their molecular dimensions and polarity (Supplementary Table S1) lead to variations in adsorption behavior across different PAC types.

Microporosity was key to the adsorption capacity and affinity for both compounds in this study. PAC-4 showed the best uptake of MIB (Qe = 73.75 ng/mg) and geosmin (Qe = 77.17 ng/mg) at a 3 mg/L PAC dosage (Figures 2a,b). This is due to its predominant pore fraction in the 0.54–1.0 nm range (0.1512 cm³/g), which aligns with



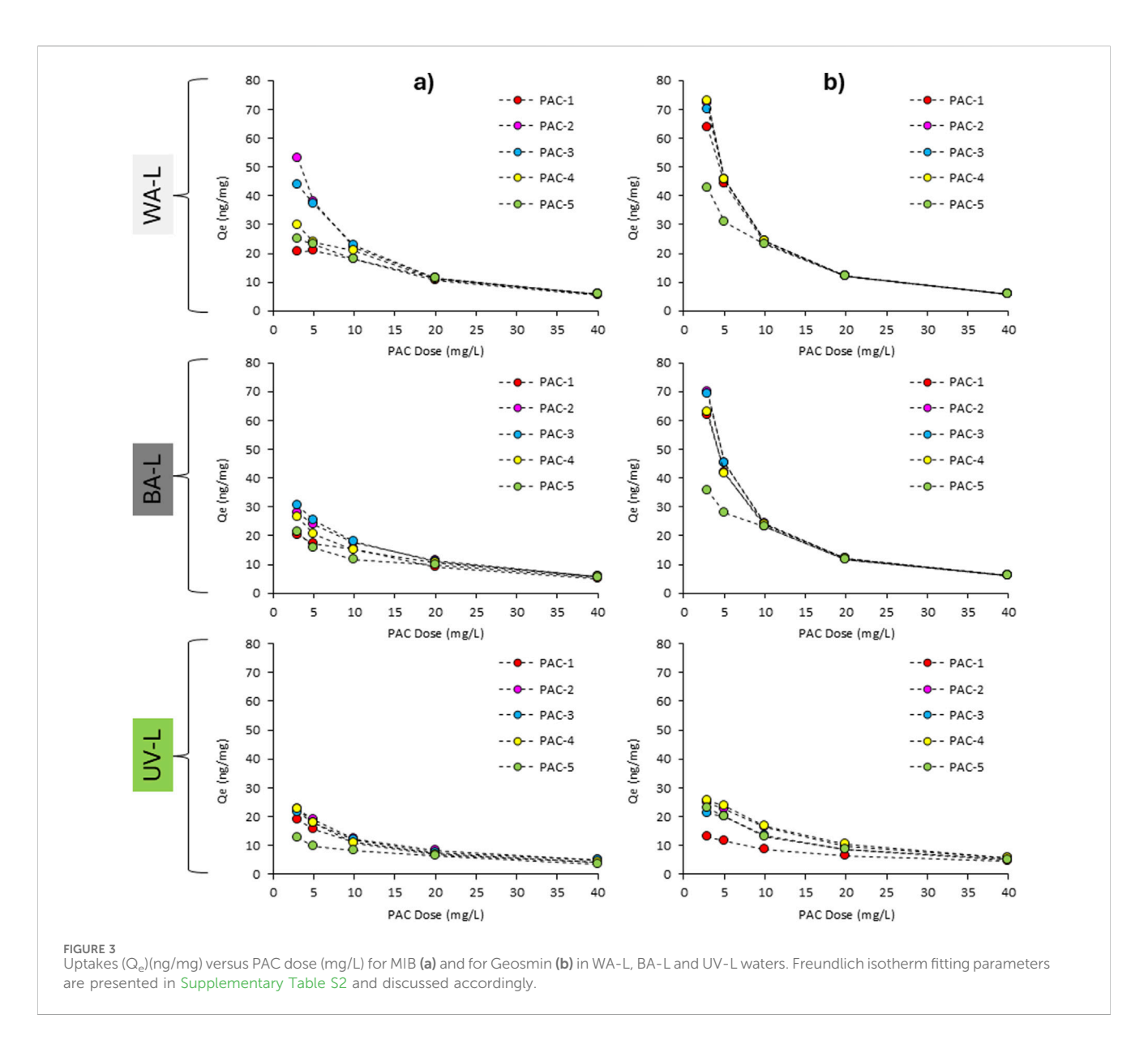
the diameters of MIB and Geosmin. These results support previous studies highlighting the importance of narrow micropores (<1.2 nm) in the adsorption of small, hydrophobic compounds (Ma et al., 2019; Newcombe, 1999; Newcombe et al., 2002a; Pelekani and Snoeyink, 1999; Zhang et al., 2011). PAC-1 showed strong uptake of both compounds. This aligns with its extensive BET surface area of 1708 m²/g and significant micropore volume. Although PAC-1 has a micropore volume like that of PAC-4, its wider pores (1-2 nm) may cause lower confinement energy and weaker interactions with MIB and Geosmin. PAC-3, despite having a smaller BET and micropore volume than PAC-1, achieved comparable Qe values-70.93 ng/mg for MIB and 77.30 ng/mg for geosmin compared to PAC-4. This suggests that the size of pore openings might be more important than the total micropore volume, as PAC-3 contains significant 0.54-1.0 nm pores (0.1007 cm³/g), matching the optimal adsorption range of MIB and Geosmin. PAC-5, dominated by mesoporosity (0.35 cm³/g), performed well for geosmin (Qe = 66.88 ng/mg) but lagged in MIB removal (Qe = 51.93 ng/mg). PAC-5's low micropore volume indicates weaker confinement and reduced adsorption. PAC-5's high Freundlich exponent (n = 5.03) and Kf (27.89) (Supplementary Table S2) for geosmin suggest that surface interactions may dominate under NOM-free conditions. The weaker R² values (0.88 for geosmin and 0.95 for MIB) indicate less consistent adsorption due to the heterogeneous surface. These findings show that mesopores aid transport but do not enhance the adsorption of small compounds without favorable surface chemistry (Alver et al., 2022; Ariturk, 2021; Kim et al., 2014). At 5 and 10 mg/L, PAC-4, PAC-3, and PAC-1 consistently showed higher Qe values for both compounds, highlighting the role of accessible microporosity. At 20 mg/L, the adsorption capacities converged to approximately 12 ng/mg, indicating active site saturation, thereby rendering pore structure differences less critical at higher doses.

Surface chemistry, particularly pHpzc, modulates the strength of adsorptive interactions, whereas the pore structure dictates physical accommodation. PAC-4 and PAC-3, with high pHpzc values (8.7 and 9.7), showed stronger affinities for both compounds, as indicated by higher Freundlich constants (Kf) and slope factors (n) (Supplementary Table S2). For MIB, PAC-4 had the highest Kf (30.75) and n (3.01), while for Geosmin, it showed Kf = 51.33 and

n = 2.90, with the best model fit (R² = 0.98). Surface hydrophobicity at neutral pH enhances nonpolar compound adsorption, which is consistent with the findings of Pelekani and Snoeyink, 1999, who demonstrated that hydrophobic PAC surfaces favor the removal of taste-and-odor compounds from clean water systems (Ariturk, 2021; Bong et al., 2021). PAC-2, with the lowest pHpzc (5.8), showed moderate uptake of MIB (Qe = 57.06 ng/mg) and Geosmin (Qe = 74.67 ng/mg), despite a relatively high micropore volume (~0.078 cm³/g for 0.54–1 nm, 0.19 cm³/g for 1–2 nm pore openings). The lower Freundlich constants (MIB: Kf = 6.68; geosmin: Kf = 21.82) and weaker R² values (0.99 for MIB, 0.85 for geosmin) indicate that surface polarity may reduce the affinity, particularly for geosmin, which is slightly more polar than MIB (Ariturk, 2021; Bong et al., 2021; Guo et al., 2008).

Freundlich fitting model results (Supplementary Table S2) showed heterogeneous surface adsorption for both compounds. For MIB, best fits were PAC-2 ($R^2=0.99$), PAC-4 ($R^2=0.98$), and PAC-3 ($R^2=0.84$). For Geosmin, PAC-4 led ($R^2=0.98$), followed by PAC-3 ($R^2=0.95$) and PAC-1 ($R^2=0.89$). Strong fits indicate multilayer adsorption or variable energy sites typical of PACs. High Kf values (PAC-4: 30.75 for MIB, 51.33 for Geosmin) and n values (>2) show favorable adsorption. The better PAC performance for Geosmin over MIB—despite Geosmin's size—is notable. This may be due to its higher hydrophobicity in the absence of NOM competition.

In summary, in the absence of NOM, PAC-4 exhibited the highest adsorption capacity and affinity owing to its ideally arranged pore structure and advantageous surface characteristics. PAC-3 exhibited high performance, indicating its efficiency, despite its relatively low BET surface area. While PAC-1's high BET surface area contributed to good uptake, its less optimized pore size limited its performance. PAC-5 was less effective due to insufficient microporosity or less favorable surface chemistry. These findings align with the literature, which emphasizes the importance of narrow micropores and hydrophobic surfaces for the effective removal of trace-level compounds (Newcombe, 1999; Pelekani and Snoeyink, 1999). The results collectively indicate that microporous PACs with sufficient and accessible pore volumes (pore openings of 0.54–2), along with a higher pHpzc, provide optimal accessibility and confinement for both MIB and Geosmin.



3.4 Impact of NOM on MIB and geosmin uptake

The influence of NOM origin and composition on MIB and Geosmin adsorption was evaluated by analyzing the adsorption behavior across three water types: WA-L, BA-L, and UV-L, each containing ~7.5 mg/L DOC (Figure 3). Despite identical DOC concentrations, the adsorption performance varied significantly owing to the NOM characteristics, specifically the SUVA $_{254}$ and E2/E3 ratios, which indicate aromaticity and molecular weight, respectively. With a high E2/E3 ratio (13.5) and moderate SUVA $_{254}$ (3.38 L/mg·m), WA-L suggests aromatic and low-MW NOM characteristics. BA-L, with an intermediate E2/E3 ratio (8.5) and moderate SUVA $_{254}$ (2.66), indicates transitional NOM, which is more humified than WA-L, yet more aromatic than UV-L. UV-L, with a low E2/E3 ratio (5.6) and lower SUVA $_{254}$ (2.22), reflects less aromatic, higher-MW fulvic-like substances (Table 1).

The compositional differences among the NOM sources significantly influenced the adsorption behavior (Figure 3). UV-

L caused the most significant reduction in MIB and Geosmin uptake across PACs (Figures 3a,b). PAC-4's Geosmin Qe decreased from 77.17 ng/mg (NOM-free) to 25.4 ng/mg in UV-L, while its MIB Qe dropped from 73.75 to 22.6 ng/mg under the same conditions. Despite UV-L's low SUVA₂₅₄ and low E2/ E3 ratio, indicating higher MW and less aromatic fulvic-like structures, which block PAC micropores or form surface films, limiting adsorption sites. Physical pore-blocking dominates the interference mechanism of UV-L rather than direct chemical competition. The highest E2/E3 ratio and moderate SUVA₂₅₄, reflecting low-MW but relatively aromatic NOM (WA-L), caused the least suppression. Although WA-L contains small aromatic moieties, they may be structurally unsuited for effective micropore competition. PAC-4 maintained high uptake in WA-L conditions (MIB Qe = 29.7 ng/mg; Geosmin Qe = 72.9 ng/mg) (Figures 3a,b), indicating that WA-L NOM did not significantly hinder micropore access. BA-L exhibited moderate suppression with intermediate E2/E3 and SUVA254 values, consistent with its partially humified character. BA-L contains

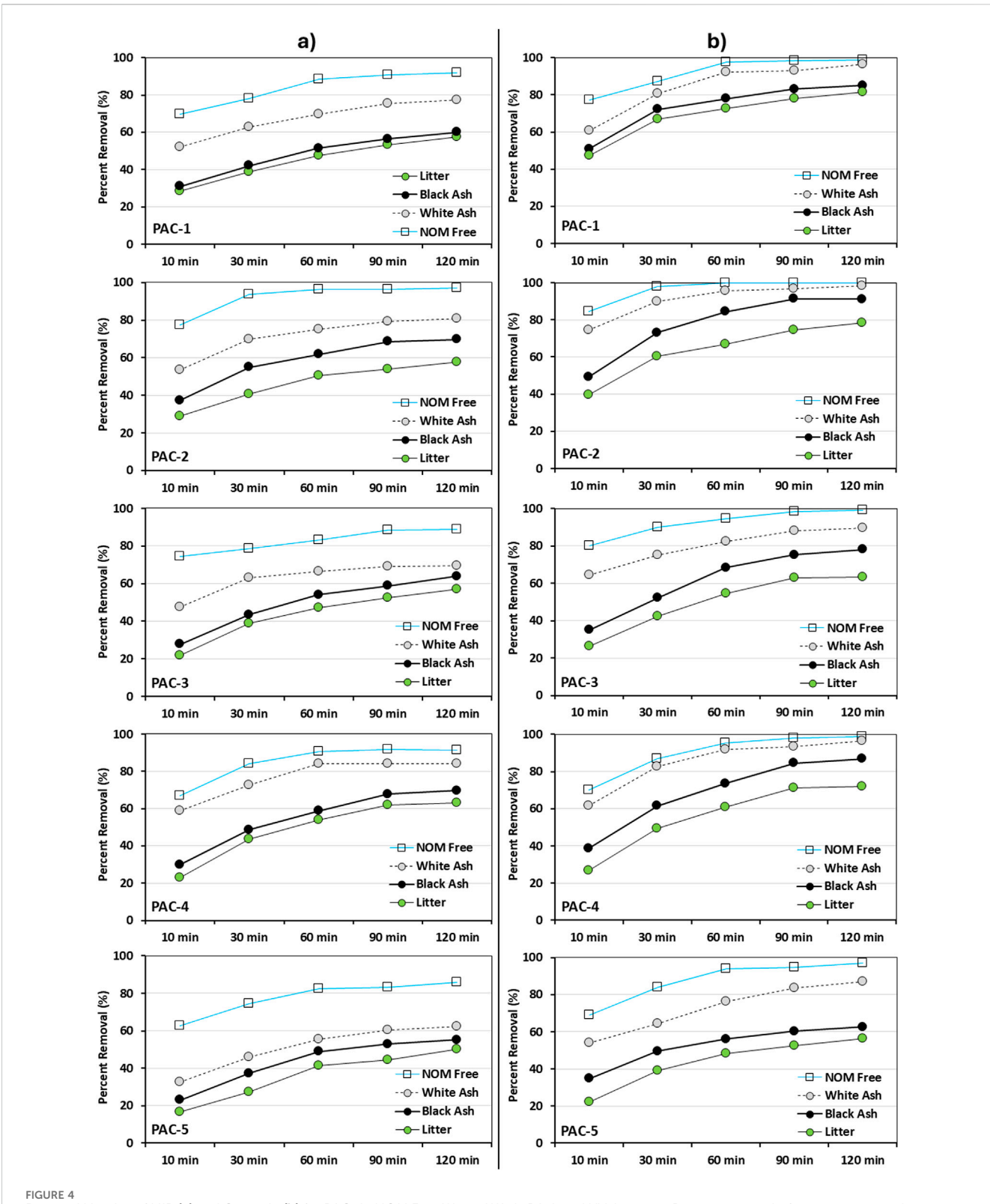


FIGURE 4
Removal kinetics of MIB (a) and Geosmin (b) for PACs in NOM Free Water, WA-L, BA-L and UV-L waters. Percent removal of target compounds as a function of contact time (10–120 min) of PACs. NOM-free water is shown as blue lines with open squares, WA-L as black dashed lines with grey circles, BA-L as solid black lines with black filled circles, and UV-L as solid black lines with filled green circles.

mid-sized aromatic compounds capable of entering micropores, reducing adsorption efficiency. PAC-3 and PAC-4 experienced notable declines in Qe for both compounds. Freundlich constants

(Kf) were approximately halved in BA-L compared to those in NOM-free waters, reflecting this intermediate competition (Supplementary Table S2).

frontiersin.org

These findings confirm that NOM suppression depends on a combination of the MW, conformation, and polarity. UV-L had larger and more disruptive molecules, whereas WA-L allowed relatively unimpeded PAC performance owing to structural incompatibility or low hydrophobicity (Newcombe et al., 2002b; Newcombe et al., 2002a; Pelekani and Snoeyink, 1999). The suppression trend was UV-L > BA-L > WA-L, with implications for PAC selection in post-fire NOM conditions. At lower PAC doses (3 and 5 mg/L), NOM impact was significant, varying performance based on PAC properties and NOM type. PAC-4 and PAC-3, which had well-aligned micropores and hydrophobic surfaces, consistently outperformed the others under competitive NOM conditions. At 10 mg/L, the uptake efficiency improved across all PACs and NOM types, although adsorption suppression remained evident in UV-L. At a 20 mg/L PAC dose, the Qe values converged across all PACs and NOM types, reaching 11-12 ng/mg for both MIB and Geosmin (Figures 3a,b). High PAC doses can overcome NOM-induced limitations by saturating competitive sites or providing an abundant, accessible surface area. The previous studies also confirm that PAC removal of organic micropollutants is dose-dependent, especially for hydrophobic compounds like MIB and geosmin (Campinas et al., 2021; Rodriguez et al., 2016). While not cost-effective for routine treatment, this threshold offers operational guidance during bloom events when NOM loading is elevated.

Although MIB and Geosmin have similar molecular size and hydrophobicity, Geosmin showed lower susceptibility to NOM interference. In UV-L waters, Geosmin Qe decreased more than MIB in most PACs, likely due to Geosmin's slightly higher hydrophobicity (log Kow ≈ 3.6 vs. 3.3 for MIB), enhancing competitive interactions with hydrophobic NOM components. Geosmin uptakes were consistently higher in all conditions, indicating a stronger affinity for hydrophobic PAC surfaces. Freundlich isotherm modeling confirms these findings. Geosmin exhibited higher Kf and n values across the PACs (Supplementary Table S2), indicating favorable adsorption. MIB showed similar trends but lower affinity constants under NOM competition. The steeper isotherms of geosmin (n > 2.8) indicate a higher uptake efficiency at low concentrations without interference.

This study revealed the complex interplay between PAC characteristics, NOM characteristics, and PAC dose. PAC-4 exhibited the most consistent performance, which was attributed to its microporosity (ranging from 0.54–1 nm to 1–2 nm) and high pHpzc of 8.7. While ash-derived NOMs influenced adsorption, the most significant competitive or pore-blocking effects were noted in UV-L water. This suggests that higher-MW compounds can more effectively reduce uptake than their lower-MW ash-derived counterparts.

3.5 Adsorption kinetics of MIB and geosmin in NOM-free water

Isotherm experiments showed that MIB and Geosmin uptake varied among adsorbents at lower PAC doses (3–10 mg/L). However, at a PAC dose of 20 mg/L, the removal efficiencies were consistent across all PAC types and water backgrounds. This confirmed that 20 mg/L was sufficient for both compounds to reach near-optimal removal levels. Therefore, adsorption kinetics

from 10 to 120 min were evaluated using 20 mg/L of each PAC, with initial MIB and Geosmin concentrations maintained at 100 ± 5 ng/L in NOM-free water.

Figures 4a, b present the kinetic removal profiles of MIB and Geosmin, respectively, across all experimental conditions, including NOM-free water and the three leachate waters (UV-L, BA-L, and WA-L). Across all PACs, more than 80% of MIB and over 90% of geosmin uptake occurred within the first 60 min, indicating rapid adsorption kinetics under non-competitive conditions. Geosmin was consistently adsorbed more rapidly than MIB, which aligns with its higher hydrophobicity (log Kow≈ 3.6 vs. 3.3 for MIB) and favorable molecular structure for interaction with slit-shaped micropores (Newcombe et al., 2002a; Karanfil and Kilduff, 1999). Performance differences were evident within the first 10 min. PAC-2, a bituminous coal-based PAC with a balanced micropore distribution in the 1-2 nm range (0.1925 cm³/g), exhibited the fastest kinetics, removing 77.4% of MIB and 84.6% of geosmin. PAC-1, a wood-based PAC with the highest BET surface area (1708 m²/g) and high mesopore volume (0.79 cm³/g), followed closely with 70.1% MIB and 77.5% geosmin removal. PAC-3 and PAC-4 exhibited moderate early-stage performance, achieving approximately 65%-75% removal of both compounds. Simultaneously, PAC-5, with the lowest micropore volume (0.0923 cm³/g) and surface area (523 m²/g), lagged with only 63.0% MIB and 68.9% geosmin removal at 10 min. At the 30min mark, the performance trend remained consistent. PAC-2 again led, achieving 93.6% MIB and 98.1% geosmin removal, followed by PAC-1, PAC-3, and PAC-4, each removing 78%-85% of MIB and 87%-90% of geosmin. PAC-5 remained the poorest performer, with ~75% MIB and ~84% geosmin removal at 30 min. These results emphasize that the 1-2 nm micropore fraction enables fast and accessible adsorption pathways for the target molecules. By 120 min, most PACs (except PAC-5) had reached near-complete removal, with ≥91% MIB and ≥98.5% geosmin removal. PAC-2 ranked highest again, achieving 97.2% MIB and 100% geosmin removal. PAC-1 performed similarly well, removing 92.0% of MIB and 98.6% of geosmin, facilitated by its extensive mesopore network and highest total micropore volume in the 0.54-2 nm range (0.3009 cm³/g). PAC-3 and PAC-4 showed similar results, with 88.9 and 91.3 percent MIB and 99 percent geosmin removal, respectively. PAC-5, on the other hand, although showing improvements over time, was the least efficient, with 86.1 percent MIB and 96.9 percent removal of geosmin, due to its limited micropore volume and surface area.

The findings align with kinetic modeling of PFOs, which indicates higher rate constants for geosmin compared to MIB across all PACs (Supplementary Table S3). Geosmin adsorbs more rapidly than MIB due to its greater hydrophobicity and superior fit into micropores. The most effective adsorbent, PAC-2, exhibited rate constants of 0.19122 min⁻¹ for MIB and 0.31534 min⁻¹ for geosmin, reinforcing the idea of its higher adsorption affinity. This supports the conclusion that the removal was driven not only by concentration gradients but also by the favorable availability of sorption sites and the micropore accessibility of the adsorbent. The rate constants derived from this model followed the sequence PAC-2>PAC-1>PAC-3≈PAC-4> PAC-5, reflecting the observed 10–30-min removals. These results collectively confirm that: i) rapid and high adsorption

frontiersin.org

kinetics are most closely correlated with micropore volume in the 0.54–2 nm range, particularly 1–2 nm pores that offer both accessibility and faster adsorption potential; ii) mesoporosity enhances diffusion rates, particularly in the early stages of adsorption, but final performance depends more on micropore accessibility and connectivity; and iii) BET surface area alone is not predictive of performance; instead, the distribution and accessibility of functional pore sizes are critical for effectively removing small, trace-level compounds such as MIB and Geosmin.

3.6 Kinetics in the presence of NOM

NOM significantly affected MIB and Geosmin adsorption kinetics, with suppression varying by NOM type. Measurements at 10, 30, and 120 min showed that NOM impacted the adsorption rate and extent across PACs, following the order: UV-L > BA-L > WA-L. This suppression hierarchy corresponded with the NOM characteristics, including the SUVA $_{254}$ and E2/E3 ratios. UV-L, with high SUVA $_{254}$ and low E2/E3, contains larger aromatic macromolecules that foul PAC surfaces, whereas WA-L, with low SUVA $_{254}$ and high E2/E3, comprises smaller hydrophilic and sterically excluded NOM fractions.

At 10 min, NOM showed measurable kinetic suppression. PAC-1, with a high BET surface area (1708 m²/g) and mesopore volume (0.79 cm³/g), achieved 70.1% removal of MIB and 77.5% of Geosmin in NOM-free water. Under UV-L conditions, these rates decreased to 53.5% and 61.2%, respectively. These reductions indicate rapid external fouling, particularly in PACs with open mesoporous structures. PAC-2 and PAC-4, featuring tighter micropore networks (0.2711 and 0.2955 cm³/g in 0.54-2 nm pores), showed slower but stable performance, resisting pore blockage owing to limited mesoporosity and narrower entrance pores. At 30 min, the suppression effects intensified. Under UV-L, PAC-4's removal of Geosmin and MIB decreased from 90.6% to 84.2% (NOMfree) to 68.4% and 55.9%, while PAC-3, with a balanced micromesopore profile (0.2189 cm³/g in 0.54-2 nm range), decreased from 85.7% to 79.6%-62.3% and 50.1%. This indicates that UV-L induces surface fouling (blocking pores) and hinders diffusion (Karanfil and Kilduff, 1999; Newcombe, 1999; Zhang et al., 2011), especially in PACs with external mesopores such as PAC-1 and PAC-3. At 120 min, the differences across the NOM types peaked. Under UV-L, PAC-4's geosmin removal dropped from 99% to 75.4%, and MIB from 91% to 62.4%. Under BA-L, Geosmin and MIB removal fell to 83.0% and 68.2%, respectively, showing competition for micropores by lower molecular weight aromatic NOM. With higher E2/E3 and lower SUVA, WA-L had the least impact due to steric exclusion: PAC-4 maintained 94% geosmin and 77% MIB removal, matching NOM-free values. PAC-2 also showed strong resilience across NOM types owing to its high micropore fraction in the 1-2 nm range (0.1925 cm³/g), providing selective access to MIB and Geosmin while restricting larger NOM components. Although PAC-2 had lower mesoporosity than PAC-1 and PAC-3, its pore geometry and narrower structure offered kinetic stability and lower fouling susceptibility. PAC-5 performed poorly, with the lowest BET surface area (523 m²/g), smallest micropore volume (0.0923 cm³/g in the 0.54-2 nm range), and limited mesopores. Its removal efficiency remained below 70% even in WA-L, highlighting the importance of micropore accessibility and surface chemistry in NOM-rich waters.

The observations confirm that the pore size distribution determines the kinetic resilience in natural waters. Micropores of 1–2 nm offer adsorption potential and partial NOM exclusion. While mesopores enable rapid uptake in NOM-free water, they become problematic under NOM exposure due to fouling, particularly under UV-L conditions. NOM type influences suppression: UV-L fouls PAC surfaces; BA-L competes within micropores; WA-L has minimal impact due to its hydrophilic, low-MW nature. Despite these challenges, all PACs—except PAC-5—achieved near-equilibrium removal (>85–90%) after 120 min in WA-L, and partially in BA-L, indicating that sufficient contact time and a PAC dose of 20 mg/L can mitigate suppression. This supports the notion that high dosing during NOM spikes (e.g., post-wildfire runoff) can overcome kinetic barriers and site competition (Qeq \approx 11–12 ng/mg).

PFOs confirmed that NOM significantly suppressed MIB and geosmin adsorption rates across all PAC types. For Example, the PFO rate constant (k) for PAC-1 decreased from 0.09823 min⁻¹ in NOM-free water to 0.00587 min⁻¹ under UV-L for MIB, showing a ~94% reduction (Supplementary Table S3). PAC-2, with the highest initial k (0.19122 min⁻¹ for MIB), experienced an 85% decrease under UV-L conditions. These reductions show that NOM, particularly UV-L with aromatic and high-SUVA fractions, impedes early-stage adsorption by fouling pore entrances or occupying adsorbent active sites. WA-L, with low SUVA₂₅₄ and high E2/E3, caused k to drop by over 60% in some PACs. These findings show PFO kinetic models capture early sorption rates and reflect NOM's impact on adsorption dynamics, especially for poorly structured PACs. Overall, results showed that the kinetic suppression across NOM types supports the idea that external fouling and competitive adsorption reduce effective diffusivity in PAC pores.

4 Conclusion and water treatment implications

This study examined the adsorption of MIB and geosmin using five different PACs under a range of NOM conditions, from wildfire ash leachates to unburned vegetation. The pore size distribution, surface chemistry, and NOM characteristics influence the effectiveness of PACs. PAC-4, characterized by narrow micropores (~0.15 cm³/g for 0.54–1 nm pore openings) and a basic surface, demonstrated the highest affinity for MIB and Geosmin both in NOM-free water and in the presence of NOM. Kinetic tests revealed that pore accessibility influenced time-dependent adsorption. The suppression of ash-derived NOM followed the order UV-L > BA-L > WA-L, based on MW and aromaticity. UV-L caused pore-blocking at early contact times, BA-L led to micropore competition, and WA-L resulted in minimal suppression.

20 mg/L PAC mitigated NOM suppression, with MIB and Geosmin uptakes converging across PAC types. This dosing threshold is a guideline for water quality disturbances, although doses may vary with DOC content. Climate change increases the frequency of wildfires globally, introducing ash-derived DOM into

source waters. These NOM forms exhibit complex compositions with high aromaticity or changed molecular weights, which pose challenges for treatment strategies. The MW of DOM determines PAC interactions and trace contaminant adsorption suppression. The findings show that PACs with micropores tailored to the dimensions of MIB and geosmin offer greater NOM interference resilience. Understanding NOM's origin and character can guide PAC selection and support integrated treatment approaches. In the realm of scientific research, future studies should utilize spectroscopic or pore analysis techniques to delve deeper into PAC–NOM interactions. This approach will help validate mechanisms such as pore fouling, hydrogen bonding, and $\pi-\pi$ interactions, as indicated by the adsorption behavior.

Data availability statement

The original contributions presented in the study are included in the article/Supplementary Material, further inquiries can be directed to the corresponding author.

Author contributions

HU: Writing – original draft, Formal Analysis, Software, Methodology, Data curation, Visualization, Conceptualization, Writing – review and editing, Validation, Investigation.

Funding

The author(s) declare that no financial support was received for the research and/or publication of this article.

Acknowledgments

The author thanks Dr. Tanju Karanfil for providing access to laboratory facilities that enabled the experimental work in this

References

Alver, A., Baştürk, E., Altaş, L., and Işık, M. (2022). A solution of taste and odor problem with activated carbon adsorption in drinking water: detailed kinetics and isotherms. *Desalination Water Treat.* 252, 300–318. doi:10.5004/dwt.2022.28269

Antonopoulou, M., Evgenidou, E., Lambropoulou, D., and Konstantinou, I. (2014). A review on advanced oxidation processes for the removal of taste and odor compounds from aqueous media. *Water Res.* 53, 215–234. doi:10.1016/j.watres.2014.01.028

Ariturk, E. (2021). Removal of 2-Methylisoborneol (MIB) and geosmin with powdered activated carbon produced from soybean. Clemson: Clemson University. Master's Thesis. Available online at: https://www.proquest.com/openview/cd49a2ebf92420af847bd08eca544d0f/1?pq-origsite=gscholar&cbl=18750&diss=y.

Belhachemi, M. (2021). "Adsorption of organic compounds on activated carbons," in Sorbents materials for controlling environmental pollution: current state and trends (Elsevier), 355–385. doi:10.1016/B978-0-12-820042-1.00006-7

Blackburn, E. A. J., Dickson-Anderson, S. E., Anderson, W. B., and Emelko, M. B. (2023). Biological filtration is resilient to wildfire ash-associated organic carbon threats to drinking water treatment. ACS ES T Water 3, 639–649. doi:10.1021/acsestwater. 2c00209

Bodí, M. B., Martin, D. A., Balfour, V. N., Santín, C., Doerr, S. H., Pereira, P., et al. (2014). Wildland fire ash: production, composition and eco-hydro-geomorphic effects. *Earth Sci. Rev.* doi:10.1016/j.earscirev.2013.12.007 study. The authors also thank Dr. Randy A. Dahlgren for providing the field samples that were essential for the leachate water generation.

Conflict of interest

The author declares that the research was conducted in the absence of any commercial or financial relationships that could be construed as a potential conflict of interest.

Generative AI statement

The author(s) declare that Generative AI was used in the creation of this manuscript. Grammatical errors were checked by AI writing agents.

Any alternative text (alt text) provided alongside figures in this article has been generated by Frontiers with the support of artificial intelligence and reasonable efforts have been made to ensure accuracy, including review by the authors wherever possible. If you identify any issues, please contact us.

Publisher's note

All claims expressed in this article are solely those of the authors and do not necessarily represent those of their affiliated organizations, or those of the publisher, the editors and the reviewers. Any product that may be evaluated in this article, or claim that may be made by its manufacturer, is not guaranteed or endorsed by the publisher.

Supplementary material

The Supplementary Material for this article can be found online at: https://www.frontiersin.org/articles/10.3389/fenvs.2025.1660425/full#supplementary-material

Bong, T., Kang, J. K., Yargeau, V., Nam, H. L., Lee, S. H., Choi, J. W., et al. (2021). Geosmin and 2-methylisoborneol adsorption using different carbon materials: isotherm, kinetic, multiple linear regression, and deep neural network modeling using a real drinking water source. *J. Clean. Prod.* 314, 127967. doi:10.1016/j.jclepro.2021.127967

Campbell, M., Treble, P. C., McDonough, L. K., Naeher, S., Baker, A., Grierson, P. F., et al. (2024). Combustion completeness and sample location determine wildfire ash leachate chemistry. *Geochem. Geophys. Geosystems* 25, e2024GC011470. doi:10.1029/2024GC011470

Campinas, M., Silva, C., Viegas, R. M. C., Coelho, R., Lucas, H., and Rosa, M. J. (2021). To what extent May pharmaceuticals and pesticides be removed by PAC conventional addition to low-turbidity surface waters and what are the potential bottlenecks? *J. Water Process Eng.* 40, 101833. doi:10.1016/j.jwpe.2020.101833

Cerón-Vivas, A., Villamizar-Leon, M. P., and Cajigas, Á. A. (2022). Geosmin and 2-Metylisoborneol removal in a drinking water treatment plant from Colombia. SSRN Electron. J. doi:10.2139/ssrn.4136275

Cerón-Vivas, A., León, M. P. V., and Cajigas, Á. A. (2023). Geosmin and 2-methylisoborneol removal in drinking water treatment. *Water Pract. Technol.* 18, 159–167. doi:10.2166/wpt.2022.167

Chen, H., Uzun, H., Chow, A. T., and Karanfil, T. (2020). Low water treatability efficiency of wildfire-induced dissolved organic matter and disinfection by-product precursors. *Water Res.* 184, 116111. doi:10.1016/j.watres.2020.116111

- Chen, H., Tsai, K. P., Liu, Y., Tolić, N., Burton, S. D., Chu, R., et al. (2021). Characterization of dissolved organic matter from wildfire-induced microcystis aeruginosa blooms controlled by copper sulfate as disinfection byproduct precursors using APPI(-) and ESI(-) FT-ICR MS. *Water Res.* 189, 116640. doi:10.1016/j.watres.2020.116640
- Chen, H., Wang, J. J., Ku, P. J., Tsui, M. T. K., Abney, R. B., Berhe, A. A., et al. (2022). Burn intensity drives the alteration of phenolic lignin to (poly) aromatic hydrocarbons as revealed by pyrolysis gas chromatography-mass spectrometry (Py-GC/MS). *Environ. Sci. Technol.* 56, 12678–12687. doi:10.1021/acs.est.2c00426
- Chen, H., Uzun, H., Tolić, N., Chu, R., Karanfil, T., and Chow, A. T. (2023). Molecular transformation of dissolved organic matter during the processes of wildfire, alum coagulation, and disinfection using ESI(–) and ESI(+) FT-ICR MS. ACS ES T Water 3, 2571–2580. doi:10.1021/acsestwater.3c00135
- Cook, D., and Newcombe, G. (2004). "Can we predict the removal of MIB and geosmin with PAC by using water quality parameters?," in *Water science and technology: water supply*. doi:10.2166/ws.2004.0081
- Cook, D., Newcombe, G., and Sztajnbok, P. (2001). The application of powdered activated carbon for mib and geosmin removal: predicting pac doses in four raw waters. *Wat. Res.* 35, 1325–1333. doi:10.1016/s0043-1354(00)00363-8
- Dastgheib, S. A., Karanfil, T., and Cheng, W. (2004). Tailoring activated carbons for enhanced removal of natural organic matter from natural waters. *Carbon N. Y.* 42, 547–557. doi:10.1016/j.carbon.2003.12.062
- De Palma-Dow, A., McCullough, I. M., and Brentrup, J. A. (2022). Turning up the heat: long-Term water quality responses to wildfires and climate change in a hypereutrophic Lake. *Ecosphere* 13, e4271. doi:10.1002/ecs2.4271
- Doederer, K., De Vera, G. A., Espino, M. P., Pype, M. L., Gale, D., and Keller, J. (2018). MIB and geosmin removal during adsorption and biodegradation phases of GAC filtration. *Water Supply* 18, 1449–1455. doi:10.2166/ws.2017.213
- Emelko, M. B., Silins, U., Bladon, K. D., and Stone, M. (2011). Implications of land disturbance on drinking water treatability in a changing climate: demonstrating the need for "source water supply and protection" strategies. *Water Res.* 45, 461–472. doi:10.1016/j.watres.2010.08.051
- Feller, M. C. (2005). Forest harvesting and streamwater inorganic chemistry in Western North America: a review. *J. Am. Water Resour. Assoc.* 41, 785–811. doi:10. 1111/j.1752-1688.2005.tb03771.x
- Ferrer, I., Thurman, E. M., Zweigenbaum, J. A., Murphy, S. F., Webster, J. P., and Rosario-Ortiz, F. L. (2021). Wildfires: identification of a new suite of aromatic polycarboxylic acids in ash and surface water. *Sci. Total Environ.* 770, 144661. doi:10.1016/j.scitotenv.2020.144661
- Gagliano, E., Falciglia, P. P., Zaker, Y., Karanfil, T., and Roccaro, P. (2021). Microwave regeneration of granular activated carbon saturated with PFAS. *Water Res.* 198, 117121. doi:10.1016/i.watres.2021.117121
- Gleasman, G., Mo, X., Atkins, J. W., Hagan, D., Campbell, B. J., Patabandige, D. L. J., et al. (2025). Postfire biogeochemical processes: implications to source water quality in fire-influenced watersheds. *Environ. Sci. Technol.* 59, 14767–14779. doi:10.1021/acs.est.4c11860
- Guo, Y., Kaplan, S., and Karanfil, T. (2008). The significance of physical factors on the adsorption of polyaromatic compounds by activated carbons. *Carbon N. Y.* 46, 1885–1891. doi:10.1016/j.carbon.2008.07.032
- Gustine, R. N., Hanan, E. J., Robichaud, P. R., and Elliot, W. J. (2022). From burned slopes to streams: how wildfire affects nitrogen cycling and retention in forests and fire-prone watersheds. *Biogeochemistry* 157, 51–68. doi:10.1007/s10533-021-00861-0
- Hampton, T. B., Lin, S., and Basu, N. B. (2022). Forest fire effects on stream water quality at Continental scales: a meta-analysis. *Environ. Res. Lett.* 17, 064003. doi:10. 1088/1748-9326/ac6a6c
- Karanfil, T., and Kilduff, J. E. (1999). Role of granular activated carbon surface chemistry on the adsorption of organic compounds. 1. Priority pollutants. *Environ. Sci. Technol.* 33, 3217–3224. doi:10.1021/es981016g
- Kim, K. T., and Park, Y. G. (2021). Geosmin and 2-MIB removal by full-scale drinkingwater treatment processes in the Republic of Korea. *WaterSwitzerl.* 13, 628. doi:10.3390/w13050628
- Kim, C., Lee, S.Il, Hwang, S., Cho, M., Kim, H. S., and Noh, S. H. (2014). Removal of geosmin and 2-methylisoboneol (2-MIB) by membrane system combined with powdered activated carbon (PAC) for drinking water treatment. *J. Water Process Eng.* 4, 91–98. doi:10.1016/j.jwpe.2014.09.006
- Klausen, M. M., and Grønborg, O. (2010). Pilot scale testing of advanced oxidation processes for degradation of geosmin and MIB in recirculated aquaculture. *Water Sci. Technol. Water Supply* 10, 217–225. doi:10.2166/ws.2010.246
- Lee, E. S., Kim, Y. N., Kim, S. B., Jung, J. S., Cha, Y. S., and Kim, B. S. (2020). Distribution and characteristics of geosmin and 2-MIB-producing actinobacteria in the Han River, Korea. *Water Sci. Technol. Water Supply* 20, 1975–1987. doi:10.2166/ws.2020.110
- Ma, L., Peng, F., Li, H., Wang, C., and Yang, Z. (2019). Adsorption of geosmin and 2-methylisoborneol onto granular activated carbon in water: isotherms, thermodynamics, kinetics, and influencing factors. *Water Sci. Technol.* 80, 644–653. doi:10.2166/wst. 2019 284
- Majidzadeh, H., Chen, H., Coates, T. A., Tsai, K.-P., Olivares, C. I., Trettin, C., et al. (2019). Corrigendum: long-term watershed management is an effective strategy to

- reduce organic matter export and disinfection by-product precursors in source water. Int. J. Wildland Fire 28, 804–813. doi:10.1071/WF18174
- Majidzadeh, H., Uzun, H., Chen, H., Bao, S., Tsui, M.T.-K., Karanfil, T., et al. (2020). Hurricane resulted in releasing more nitrogenous than carbonaceous disinfection byproduct precursors in coastal watersheds. *Sci. Total Environ.* 705, 135785. doi:10. 1016/j.scitotenv.2019.135785
 - Marden, A. (2020). Geospatial analysis of the 2020 LNU lightning complex fires.
- Matsui, Y., Aizawa, T., Kanda, F., Nigorikawa, N., Mima, S., and Kawase, Y. (2007). Adsorptive removal of geosmin by ceramic membrane filtration with super-powdered activated carbon. *J. Water Supply Res. Technol. AQUA* 56, 411–418. doi:10.2166/aqua.2007.017
- Matsui, Y., Nakao, S., Taniguchi, T., and Matsushita, T. (2013). Geosmin and 2-methylisoborneol removal using superfine powdered activated carbon: shell adsorption and branched-pore kinetic model analysis and optimal particle size. *Water Res.* 47, 2873–2880. doi:10.1016/j.watres.2013.02.046
- Mustapha, S., Tijani, J. O., Ndamitso, M., Abdulkareem, A. S., Shuaib, D. T., and Mohammed, A. K. (2021). A critical review on geosmin and 2-methylisoborneol in water: sources, effects, detection, and removal techniques. *Environ. Monit. Assess.* 193, 204. doi:10.1007/s10661-021-08980-9
- Newcombe, G. (1999). Charge vs. porosity some influences on the adsorption of natural organic matter (NOM) by activated carbon. *Water Sci. Technol.* 40, 191–198. doi:10.2166/wst.1999.0474
- Newcombe, G., Morrison, J., Hepplewhite, C., and Knappe, D. R. U. (2002a). "In the (adsorption) competition between NOM and MIB, who is the winner, and why?," in *Water science and technology: water supply.* doi:10.2166/ws.2002.0046
- Newcombe, G., Morrison, J., Hepplewhite, C., and Knappe, D. R. U. (2002b). Simultaneous adsorption of MIB and NOM onto activated carbon. *Carbon N. Y.* 40, 2147–2156. doi:10.1016/S0008-6223(02)00098-2
- NCCI, (2020). Coordination Center (NICC) Wildland Fire Summary and Statistics Annual Report. Available online at: https://www.nifc.gov/sites/default/files/NICC/2-Predictive%20Services/Intelligence/Annual%20Reports/2020/annual_report_0.pdf
- Otten, T. G., Graham, J. L., Harris, T. D., and Dreher, T. W. (2016). Elucidation of tasteand odor-producing bacteria and toxigenic Cyanobacteria in a Midwestern drinking water supply reservoir by shotgun metagenomic analysis. *Appl. Environ. Microbiol.* 82, 5410–5420. doi:10.1128/AEM.01334-16
- Park, S. M., Heo, T. Y., Park, N. B., Na, K. J., Jun, H. B., and Jung, J. Y. (2010). Application of air stripping to powdered activated carbon adsorption of geosmin and 2-methylisoborneol. J. Water Supply Res. Technol. - AQUA 59, 492–500. doi:10.2166/aqua.2010.101
- Paul, M. J., LeDuc, S. D., Lassiter, M. G., Moorhead, L. C., Noyes, P. D., and Leibowitz, S. G. (2022). Wildfire induces changes in receiving waters: a review with considerations for water quality management. *Water Resour. Res.* 58, e2021WR030699. doi:10.1029/2021WR030699
- Peak, C. (2025). National interagency coordination center wildland fire summary and statistics annual report 2020.
- Pelekani, C., and Snoeyink, V. L. (1999). Competitive adsorption in natural water: role of activated carbon pore size. *Water Res.* 33, 1209–1219. doi:10.1016/S0043-1354(98) 00329-7
- Pochiraju, S., Hoppe-Jones, C., Weinrich, L., Maalouf, S., and Adams, C. (2022). Treatability of 18 taste and odor compounds using powdered activated carbon in drinking water utilities. *AWWA Water Sci.* 4, e1289. doi:10.1002/aws2.1289
- Qiu, P., Zhang, Y., Mi, W., Song, G., and Bi, Y. (2023). Producers and drivers of odor compounds in a large drinking-water source. *Front. Ecol. Evol.* 11, 1216567. doi:10. 3389/fevo.2023.1216567
- Richardson, C., Montalvo, M., Wagner, S., Barton, R., Paytan, A., Redmond, M., et al. (2024). Exploring the complex effects of wildfire on stream water chemistry: insights from concentration-discharge relationships. *Water Resour. Res.* 60, e2023WR034940. doi:10.1029/2023WR034940
- Rodriguez, E., Campinas, M., Acero, J. L., and Rosa, M. J. (2016). Investigating PPCP removal from wastewater by powdered activated Carbon/Ultrafiltration. *Water Air Soil Pollut*. 227, 177. doi:10.1007/s11270-016-2870-7
- Silins, U., Stone, M., Emelko, M. B., and Bladon, K. D. (2009). Sediment production following severe wildfire and post-fire salvage logging in the Rocky Mountain headwaters of the oldman river Basin, Alberta. *Catena (Amst)* 79, 189–197. doi:10.1016/j.catena.2009.04.001
- Soyluoglu, M., Kim, D., Zaker, Y., and Karanfil, T. (2022). Removal mechanisms of geosmin and MIB by oxygen nanobubbles during water treatment. *Chem. Eng. J.* 443, 136535. doi:10.1016/j.cej.2022.136535
- Soyluoglu, M. (2023). "Nanobubble Technology for the Removal of MIB and Geosmin From Drinking Water". All Dissertations. Available online at: https://open.clemson.edu/all_dissertations/3473.
- Srinivasan, R., and Sorial, G. A. (2009a). "Treatment of microcontaminants in drinking water,". Department of Civil and Environmental Engineering of the College of Engineering.
- Srinivasan, R., and Sorial, G. A. (2009b). Adsorption of geosmin and MIB on activated carbon fibers-single and binary solute system. *Water, Air, Soil Pollut. Focus* 9, 223–235. doi:10.1007/s11267-009-9217-y

Srinivasan, R., and Sorial, G. A. (2011). Treatment of taste and odor causing compounds 2-methyl isoborneol and geosmin in drinking water: a critical review. *J. Environ. Sci.* 23, 1–13. doi:10.1016/S1001-0742(10)60367-1

Srinivasan, R., Sorial, G. A., Ononye, G., Husting, C., and Jackson, E. (2008). Elimination of persistent odorous compounds from drinking water. *Water Sci. Technol. Water Supply* 8, 121–127. doi:10.2166/ws.2008.057

Szczurek, A., Maciejewska, M., Kabsch-Korbutowicz, M., Wolska, M., and Solipiwko-Pieścik, A. (2024). Geosmin and 2-Methylisoborneol detection in water using semiconductor gas sensors. *Electron. Switz.* 13, 63. doi:10.3390/electronics13010063

Tigerprints, T., Dissertations, A. D., and Soyluoglu, M. (2023). Nanobubble technology for the removal of MIB and geosmin nanobubble technology for the removal of MIB and geosmin from drinking water from drinking water.

Tsai, K. P., Uzun, H., Karanfil, T., and Chow, A. T. (2017). Dynamic changes of disinfection byproduct precursors following exposures of microcystis aeruginosa to wildfire ash solutions. *Environ. Sci. Technol.* 51, 8272–8282. doi:10.1021/acs.est.7b01541

Tsai, K. P., Uzun, H., Chen, H., Karanfil, T., and Chow, A. T. (2019). Control wildfire-induced microcystis aeruginosa blooms by copper sulfate: trade-Offs between reducing algal organic matter and promoting disinfection byproduct formation. *Water Res.* 158, 227–236. doi:10.1016/j.watres.2019.04.013

Uzun, H., Kim, D., and Karanfil, T. (2018). Deactivation of wastewater-derived N-nitrosodimethylamine precursors with chlorine dioxide oxidation and the effect of pH. *Sci. Total Environ.* 635, 1383–1391. doi:10.1016/j.scitotenv.2018.04.148

Uzun, H., Kim, D., and Karanfil, T. (2019). Removal of wastewater and polymer derived N-nitrosodimethylamine precursors with integrated use of chlorine and chlorine dioxide. *Chemosphere* 216, 224–233. doi:10.1016/j.chemosphere.2018.10.088

Watson, S. B., Brownlee, B., Satchwill, T., and Hargesheimer, E. E. (2000). Quantitative analysis of trace levels of geosmin and MIB in source and drinking water using headspace SPME. Water Res. 34, 2818-2828. doi:10.1016/S0043-1354(00)00027-0

Weishaar, J. L., Aiken, G. R., Bergamaschi, B. A., Fram, M. S., Fujii, R., and Mopper, K. (2003). Evaluation of specific ultraviolet absorbance as an indicator of the chemical composition and reactivity of dissolved organic carbon. *Environ. Sci. Technol.* 37, 4702–4708. doi:10.1021/es030360x

Westerhoff, P., Nalinakumari, B., and Pei, P. (2006). Kinetics of MIB and geosmin oxidation during ozonation. *Ozone Sci. Eng.* 28, 277–286. doi:10.1080/01919510600892836

Zhang, S., Shao, T., and Karanfil, T. (2011). The effects of dissolved natural organic matter on the adsorption of synthetic organic chemicals by activated carbons and carbon nanotubes. *Water Res.* 45, 1378–1386. doi:10.1016/j.watres.2010.10.023